FLUID DYNAMIC EFFECTS IN THE FUELELEMENT TOP NOZZLE AREA DURING REFILLING AND REFLOODING

A. HAWIGHORST, R. SPATZ, H.KRÖNING, D. MEWES
Institut für Verfahrenstechnik, Universität Hannover,
Bundesrepublik Deutschland
F. MAYINGER
Lehrstuhl A für Thermodynamik, Technische Universität München,
Bundesrepublik Deutschland

Summary

Counter-current flow of a gas and a liquid occurs during emergency cooling conditions in the region of downcomer and the core of ligthwater cooled nuclear reactors. In order to identify the flooding mechanisms, investigations of counter-current flow were performed under a large variety of test conditions. As internals to the flow-duct, perforated plates, a 4 x 4 rod bundle with tie plate and a complete fuel element dummy, were used to simulate hydraulically a section of the upper part of a PWR fuel element. The selected fluid systems were air-water and steam-water. During the steam-water tests the effects of subcooled water injection were also investigated.

The results of the experiments indicate similar mechanisms for counter-current flow in tubes and square ducts with and without internals. In all cases there is a distinct gradient in pressure drop and a remarkable apearance of flow instabilities near the stagnation point.

The mathematical methods leading to a flooding model are outlined. The model is based on the stability condition of the wavy interfaces. The own experimental data and those from the literature are well represented by the derived model.

1. INTRODUCTION

The knowledge about the fluiddynamic behavior of gas-liquid mixtures is an important basis of a great number of technical processes. In counter-current flow the handling of the two phases enables very often an improvement of heat and mass transfer. In general the liquid flows downwards and the gas flow is directed upwards. In the process industry the counter-current flow is used in packed columns, perforated tray columns or film evaporators. Counter-current flow of steam and water can occur also during a hypothetical emergency core cooling of light water cooled nuclear reactors. In the pressurized water reactors of the Federal Republic of Germany (FRG-PWR), two separate emergency core cooling systems are provided, which reflood the core. These are the bottom injection (cold leg injection) and the top injection (hot leg injection). From the top injection the water must pass through the upper plenum and the end-box into the core region (Fig 1). Furthermore, steam will be generated from the bottom and the top. Both coolant and steam will flow upwards through the core into the upper plenum region. The action of steam flowing upward while water flows downward can lead to a condition defined as counter-current flow limiting (CCFL), which tends to restrict the water downflow. Furthermore, water droplets will be entrained and transported by the steam flow

through the core and can deentrain in the upper plenum region. This deentrained water and the upward flowing steam can lead to the same fluid behavior discussed previously.

The purpose of the project is to investigate these mechanisms at countercurrent flow conditions in order to improve the understanding of the fluid dynamic effects during refilling and reflooding. The results should make a contribution for the improvement of the reactor computer codes, for example TRAC. In order to investigate the mentioned problem, the experimental work is split in different stages:

- Test facilities:
  - Air/Water
  - Steam/Water
- Internals:
  - Orifices and perforated plates
  - 1/16 Fuelelement (4 x 4)
  - Complete fuelelement (16 x 16)
- Optical observations of flow conditions
- Investigations of droplet entrainment
- Determination of flooding-curves
- Measurement of pressure drop

2. PHENOMENOLOGICAL DESCRIPTION OF COUNTER-CURRENT FLOW

The principle phenomenons at counter-current flow conditions are shown in Fig. 2. The lower part of the diagram gives informations about the carry-over ratio of the injected water dependent on the superficial gas velocity. At lower gas velocities all injected water flows downwards as an undisturbed annular flow. With increasing gas velocity there are greater interactions between the two phases. Waves begin to grow and become instable. Some droplets are entrained and transported upwards by the gas flow (b) . At the flooding point a considerable amount of liquid is carried out. At further increasing gas flows the carry-over ratio raises from 0 % up to 100 % (c). If the gas velocity reaches a definite value a hanging wavy film moves upwards through the flow duct and all injected water is carried out (d). At higher gas velocities there is a concurrent two phase flow above the injection and a single phase gas flow below the injection (e).

The previous discription is valid for a distinct constant water injection rate. At increasing water rates the film thickness is growing and the flow area of gas is decreasing. Therefore flooding occurs at lower gas velocities. The onset of flooding is depending on the superficial gas and water velocities. In the flooding diagram (Fig. 3) the downwards penetrating liquid is plotted versus the upwards flowing gas. The II. and IV. quadrant represent the downwards or upwards directed concurrent flow. Flow conditions in the III. quadrant, i.e. water upflow and gas downflow are physically impossible. In the I. quadrant the possible counter-current flow conditions are limited by the flooding curve. This line indicates the maximum water flow, which can penetrate downwards against a given gas flow.

3. HYDRODYNAMIC STABILITY MODEL OF FILM FLOW AT COUNTER-CURRENT FLOW

In the literature a lot of flooding models were presented. In general they can be devided in three groups, which are based on

- separated film flow models (1, 2, 3)
- instability models of surface waves (4, 5, 6, 7) and
- dimensionless numbers formed by superficial velocities (8, 9, 10, 11).

A comparison of the different models resulted, that all models do not consider the complex flow conditions in the region of the fuel element top nozzle. The parameters of the existing empirical correlations have to be adjusted to the experimental data related to different geometries.

The theory of hydrodynamic stability (12, 13) opens the possibility to extend the model conception of counter-current flow. The mathematical method is based on the stability of wavy interfaces (Fig. 4). The maximum differential velocity between the phases for a disturbance not to change the wavy boundary layer, results from the Orr-Sommerfeld equation of a frictionless flow. In order to calculate the superficial gas velocities the volumetric gas fraction is used as a parameter:

$$\frac{w_{OG}}{C\cdot\sqrt{\frac{k\cdot\sigma}{g_G}}}\cdot\frac{1}{\varepsilon}+\frac{w_{OL}}{C\cdot\sqrt{\frac{k\cdot\sigma}{g_G}}}\cdot\frac{1}{1-\varepsilon}-1=0 \qquad (1)$$

The integration constant C depends on the flow duct geometry. Fig. 5 shows a band of lines with various gas fractions. The solutions of the variation problem results in the basis equation of the flooding model, which is marked as envelope in the diagram:

$$\left(\frac{w_{OG}^2}{g}\cdot\frac{w_{OG}^2\cdot g_G}{\sigma}\cdot\frac{g_G}{(g_L-g_G)}\right)^{0,125}+M\cdot\left(\frac{w_{OL}^2}{g}\cdot\frac{w_{OL}^2\cdot g_L}{\sigma}\cdot\frac{g_L}{(g_L-g_G)}\right)^{0,125}=C \qquad (2)$$

As dimensionless numbers for both phases the Froude number, the Weber number and the density ratio are used. The equation considers the inertial, the weight and the surface forces. The influence of friction and the geometry are comprehended by parameters M and C. This dependencies are found by mean of own experiments and literature data.

The geometric parameter C is given by a hyperbolic function:

$$C = 1 + \tanh\,(Bo^*/80) \qquad (3)$$

The bond number Bo^* is defined as followed:

$$Bo^* = L\cdot\left(g\cdot\frac{(g_L-g_G)}{\sigma}\right)^{1/2} \qquad (4)$$

L is wetable parameter, an important value for the flooding behavior. A comparison in Fig. 6 shows, that the experimental data are well represented by equation 3.

The influence of friction is comprehended by an exponential equation with the viscosity ratio of the two phases.

$$\frac{M}{C} = 0{,}81\cdot\left(\frac{\nu_L}{\nu_G}\right)^{0,123} \qquad (5)$$

A comparison with experimental data is given in Fig. 7.

4. AIR WATER EXPERIMENTS

The test setup for the air-water experiments (Fig. 8) consists of an air loop and a water loop. The air is injected into the bottom of the test section after passing one of the flow element flow meters. The two phases

leaving the test section at the top are separated and the air is vented through a valve, which controls the system pressure. In the counter-current flow investigations the water is pumped into the upper part of the test section through a nozzle or porous sinter metal. The outlet mass flows - fall back and carry over - are measured by collecting tanks.

For the entrainment investigations an optical measuring device is developed, as shown in Fig. 9. The shadow photography arrangement consists of a gas flash ligth and a normal camera with an extension tube for the magnification. Weir elements near the holes of the flow duct separate the liquid film from the aperture. Droplets, entering the separating volume and wetting the windows, are removed by a small air jet and drained.

Entrainment photographs at different flow conditions are shown in the upper part of Fig. 10. The flow conditions are indicated in the carry over ratio diagram in the lower part of the figure. Increasing drop sizes with increasing air velocities can be observed. At the evalution of the droplet photographs a digital image analysing system is developed in order to get more objectiv and reproducable results of drop size distributions.

Fig. 11 shows a comparison of drop size distribution gained from single tube and bundle tests at the same air and water superficial velocities. The droplets above the tie-plate are of greater diameter. Their sizes can be explained by two quite different generating mechanisms. Typical results of the experiments with counter-current mass flow are plotted in Fig. 12. The experimental data are well represented by the derived model (Eq. 2).

5. STEAM-WATER EXPERIMENTS

An important task of the project was to investigate the fluid dynamic behavior at nearly the same flow conditions as during refilling and reflooding. Therefore a steam-water test facility was built. In the test section internals were installed up to a complete fuel element dummy. The piping and instrumentation flow sheet is shown in Fig. 13. In principal it is a similar arrangement as at the air water experiments. The maximum steam flow of 1900 kg/h can be recirculated in the test setup by a steam blower. The inlet mass flow rates are measured by different orifices and the water outlet mass flow rates are measured by collecting tanks. The system pressure is 4.8 bar (abs) corresponding to ECC-condition after the end of blow down. Fig. 14 shows the experimental results of test series with a 4 x 4 rod bundle and with the complete end box (16 x 16 rod bundle) as internal. The water is injected at saturation temperature.

Flooding can be observed at lower steam velocities in the case of the complete fuel element. At the same superficial steam velocities much less water can penetrate downwards. The main reason for this behavior is the different flow distribution in both cases. The main part of water fall back flows as a film along the flow duct wall, especially along the corners, where the local steam velocity is lower than on an average. This phenomena occurs at both geometries, but the perimeter to cross section ratio decreases with increasing sizes. Therefore the influence of the wall to the flooding behavior is much greater in smaller test sections.

With subcooled water injection an additional effect by phase changes must be considered. A part of steam flow condensates until the water attains the saturation temperature. Therefore the flooding model is extended by a term, which comprehends the steam reduction caused by condensation:

$$\left[\left(\frac{w_{OG}^2}{g}\cdot\frac{w_{OG}^2\cdot\varrho_G}{\sigma}\cdot\frac{\varrho_G}{(\varrho_L-\varrho_G)}\right)^{0,25}-f\cdot Ja\cdot\left(\frac{w_{OL,in}^2}{g}\cdot\frac{w_{OL,in}^2\,\varrho_{L,in}}{\sigma}\cdot\frac{\varrho_{L,in}}{(\varrho_{L,in}-\varrho_G)}\right)^{0,25}\right]^{0,5}$$

$$+M\cdot\left(\frac{w_{OL}^2}{g}\cdot\frac{w_{OL}^2\cdot\varrho_L}{\sigma}\cdot\frac{\varrho_L}{(\varrho_L-\varrho_G)}\right)^{0,125}=C \qquad (6)$$

M and C are the already mentioned flooding parameters, Ja is the Jakob number, $Ja = C_p\cdot\Delta T_{sub}/r$ and f gives an information about the degree of equilibrium between the phases. It depends on flow turbulences and phase interactions, on the residence time and on the flow duct geometry. The value of f can come up to a maximum of 1, i.e. all water has saturation temperature.

The flooding curves of tests with the 4 x 4 rod bundle and tie-plate as internals are presented in Fig. 15. With the same steam flow rate more water can penetrate downwards, if the injected water is subcooled. A part of the injected steam is condensed below the smallest free flow area. So the onset of flooding in this region occurs at higher steam inlet flow. The water subcooling temperature is measured in the injection tube and not at the tie-plate. Therefore the difference in flooding behavior between saturated or subcooled water injection is slight, because the water is partly heated up on its way from the injection to the smallest free flow area, which turned out to be the most important section for flooding. Only subcooled water, which attains this area, can influence the flooding behavior.

Fig. 16 shows the results of pressure drop measurements at different water injection rates. It can be observed, that with increasing steam velocities the pressure drop shows a marked maximum and approaches to the value of the single phase pressure drop at higher steam flow rates. In consequence of the mutual restrictions of gas and liquid at the onset of flooding a turbulent two phase mixture arises and the pressure drop reaches a maximum. At increasing steam velocities the considerable amount of the water is carried out and the pressure drop slightly decreases. With increasing water injection the pressure drop becomes greater and flooding takes place at lower steam velocities.

REFERENCES

1. Brauer, H.: Strömung dünner Flüssigkeitsschichten unter der Einwirkung eines angrenzenden Gasstromes. Allg. Wärmetechnik (1961)
2. Feind, K.: Strömungsuntersuchungen bei Gegenstrom von Rieselfilmen und Gas in Lotrechten Rohren. VDI-Forschungsheft 481 (1960)
3. Taitel, Y.; Bornea, D.; Dukler, A.E.: A film model for the prediction of flooding and flow reversal for gas-liquid flow in vertical tubes. Int. J. Muliphase Flow 8 (1982) 1, 1/10
4. Shearer,C.J.; Davidson, J.F.: The investigation of a standing wave due to gas blowing upwards over a liquid film; its relation to flooding in wetted-wall columns. J. Fluid Mech. 22 (1965) 2, 321/335
5. Cetinbudakler, A.G; Jameson, G.J.: The mechanism of flooding in vertical countercurrent two-phase flow. Chem. Eng. Sci. 24 (1969), 1669/1680
6. Imura, H.; Kusuda, H.; Funatsu, S.: Flooding velocity in a counter-current annular two-phase flow. Chem. Eng. Sci. 32 (1977), 79/87

7. Richter, H.J.: Flooding in tubes and annuli. Int. J. Multiphase Flow 7 (1981) 6, 647/658
8. Kutateladze, S; Sorokin, L.: The hydrodynamic stability of vapour-liquid systems. In: Problems of heat transfer and hydraulic of two-phase media. Ed. by Kutateladze, Pergamon Press, Oxford 1969, 385/395
9. Ruff, K; Pilhofer, T.; Mersmann, A.: Vollständige Durchströmung von Lochboden bei der Fluid-Dispergierung. Chem.-Ing.-Tech. 48 (1976) 9
10. Suzuki, S.; Ueda, T.: Behaviour of liquid film and flooding in counter-current two-phase flow; Part 1.Flow in circular tubes. Int. J. Multiphase Flow 3 (1977), 517/532
11. Wallis, G.B. et al.: Countercurrent gas-liquid flow in parallel vertical tubes. Int. J. Multiphase Flow 7 (1980), 1/19
12. Schlichting, H.: Grenzschichttheorie. G. Braun-Verlag, Karlsruhe (1965)
13. Wieghard, K.: Theoretische Strömungslehre. Teubner, Stuttgart (1965)

Discussion

Question: K. Wolfert - GRS

Mr. Deruaz has shown that counter current flow limitation (CCFL) occured at the upper grid plate in Pericles at a steam velocity of about 9-10 m/s (corresponding to 7-8 m/s in the core).

Did you check your model on the basis of the Pericles data, do you find any agreement?

Answer: R. Spatz - U/Hannover

We checked our model with the Pericles data.
In Pericles the counter current flow limitation is associated to a superficial steam velocity of 7-8 m/s prevailing in the core region. In our tests the superficial velocities are related to the smallest free flow area, which is the tie-plate area. In this cross section the steam velocity is nearly 20% greater. This means with respect to the Pericles data that the steam velocities are about 10 m/s.
Such velocities correspond nearly to values calculated with the model developed by us.

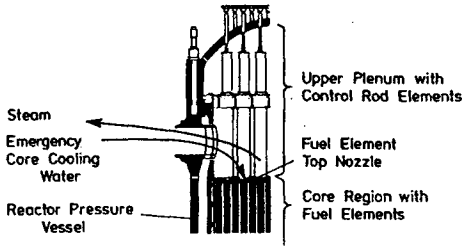

Fig. 1 Upper plenum of the reactor vessel of a PWR

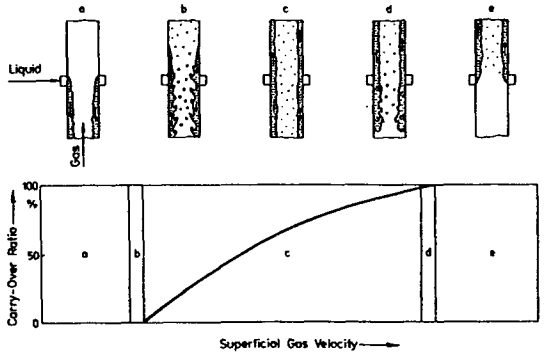

Fig. 2 Scheme of changing from concurrent to counter-current flow
a) undisturbed counter-current flow
b) onset of flooding
c) splitting of the liquid flow
d) stagnation point
e) concurrent flow upwards

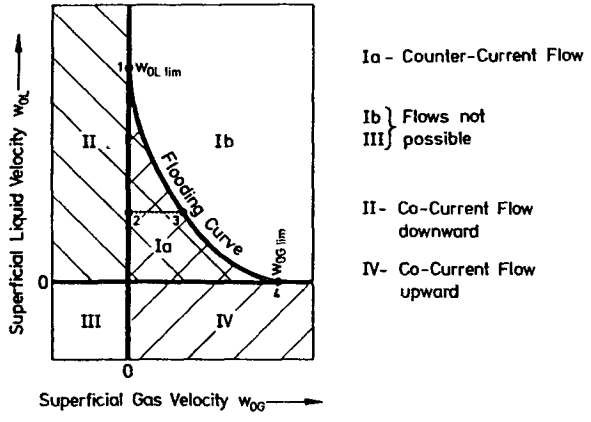

Fig. 3 Flow diagram (liquid downwards flow positiv)

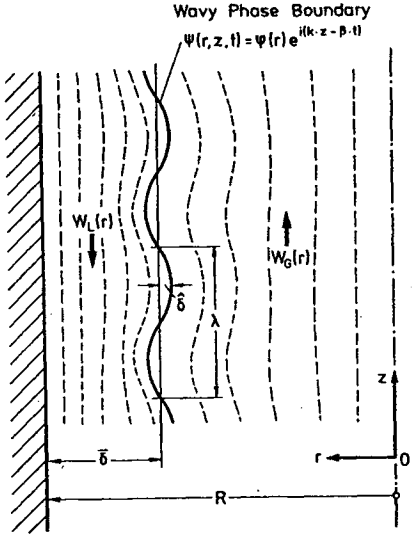

Fig. 4 Wavy interface at counter-current flow

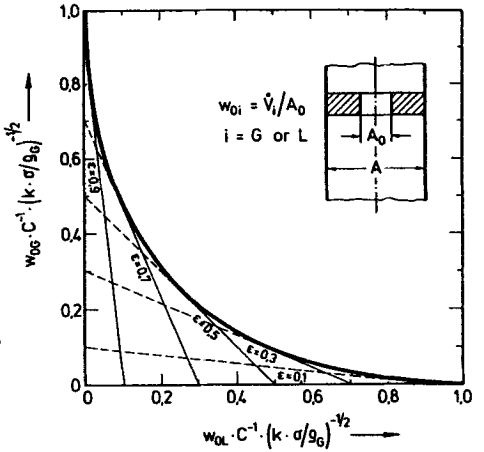

Fig. 5 Flooding function (Eq. 1)

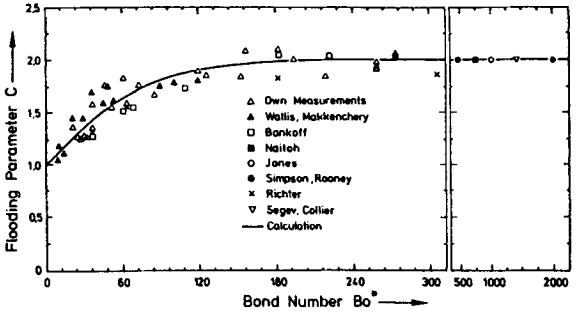

Fig. 6 Dependence of the flooding parameter C on the Bond-number (Eq. 3 + 4)

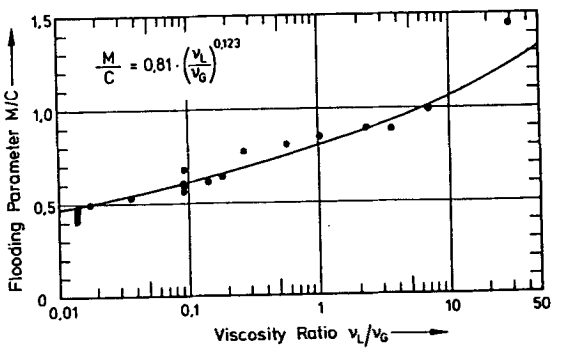

Fig. 7 Dependence of the flooding parameter M/C on the viscosity

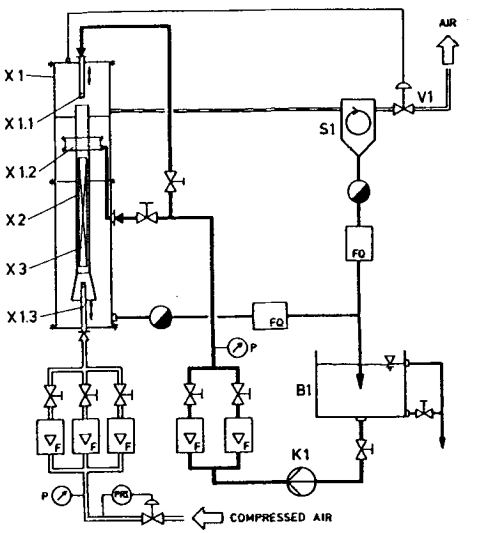

X1 Test Vessel
X1.1 Water Injection Through a Nozzle
X1.2 Water Injection Through Porous Sinter Metal
X1.3 Air Injection
X2 Flow Duct
X3 Internals
V1 Pressure Controlling System
S1 Twist Separator
B1 Water Storage Tank
K1 Centrifugal Pump

Fig. 8 Air-water test facility

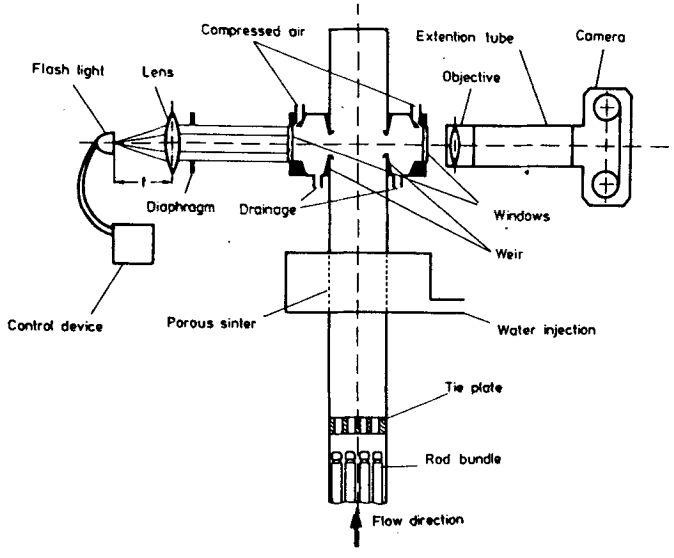

Fig. 9 Arrangement for entrainment photography

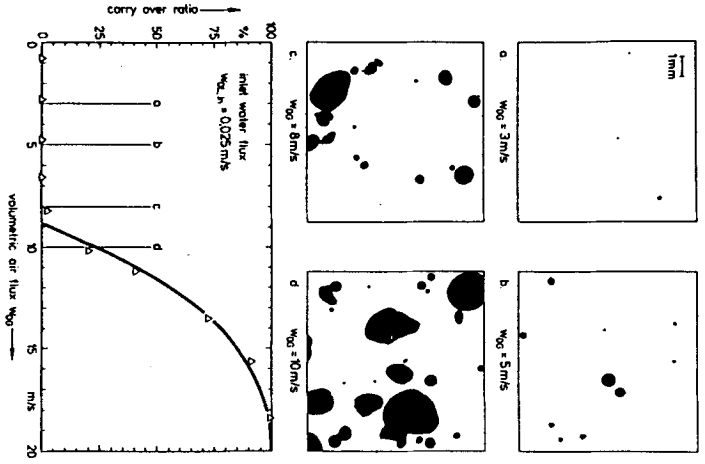

Fig. 10 Droplet photographies above the tie-plate at different superficial velocities

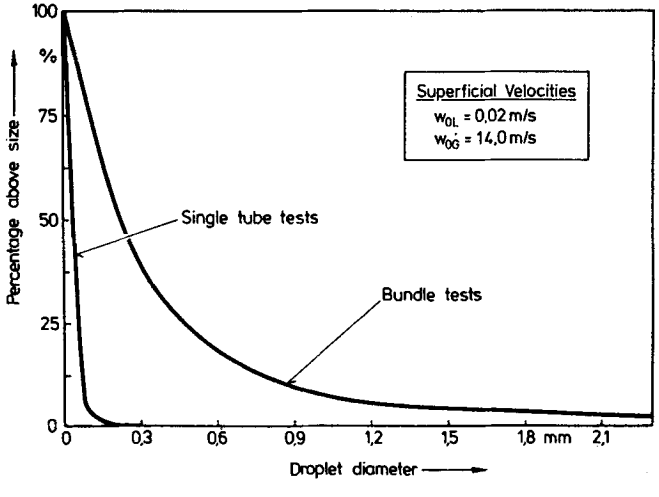

Fig. 11 Drop size distribution in a single tube and above the tie-plate

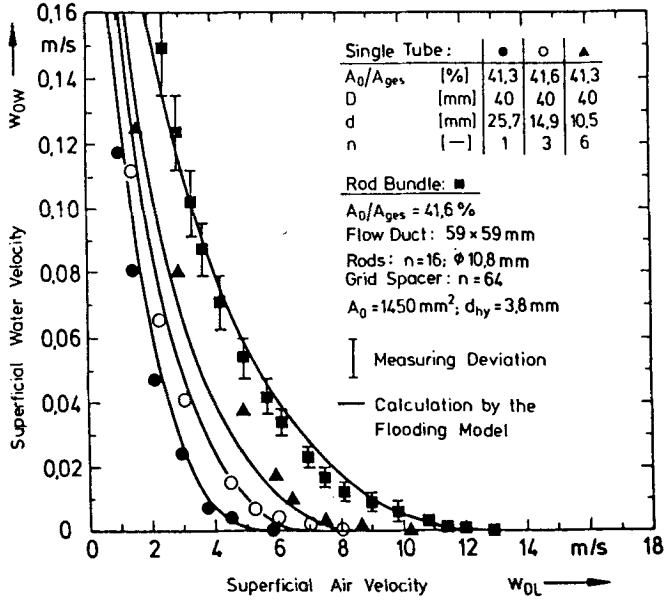

Fig. 12 Flooding behavior at different internals in the test section

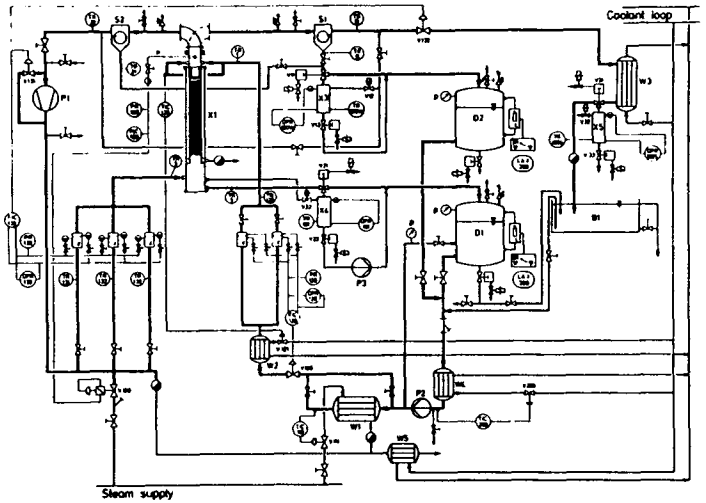

Fig. 13 Piping and instrumentation flow sheet of the steam-water loop

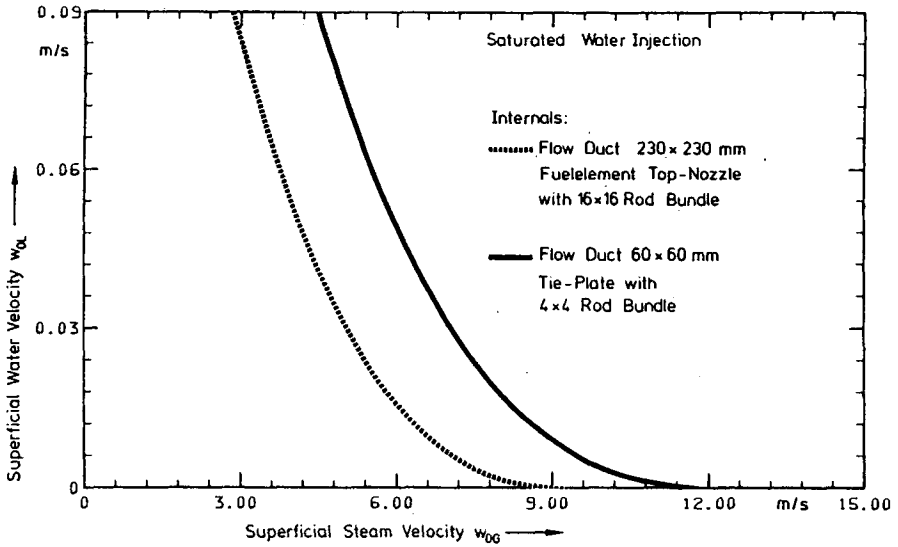

Fig. 14 Comparison of the flooding behavior for tests with the 4 x 4 and the 16 x 16 rod bundle

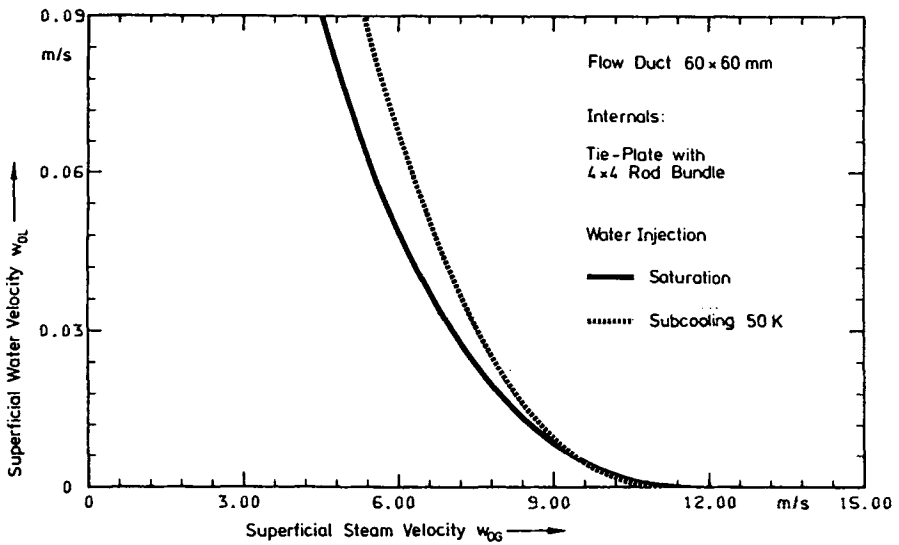

Fig. 15 Comparison of the flooding behavior at saturated and subcooled water injection

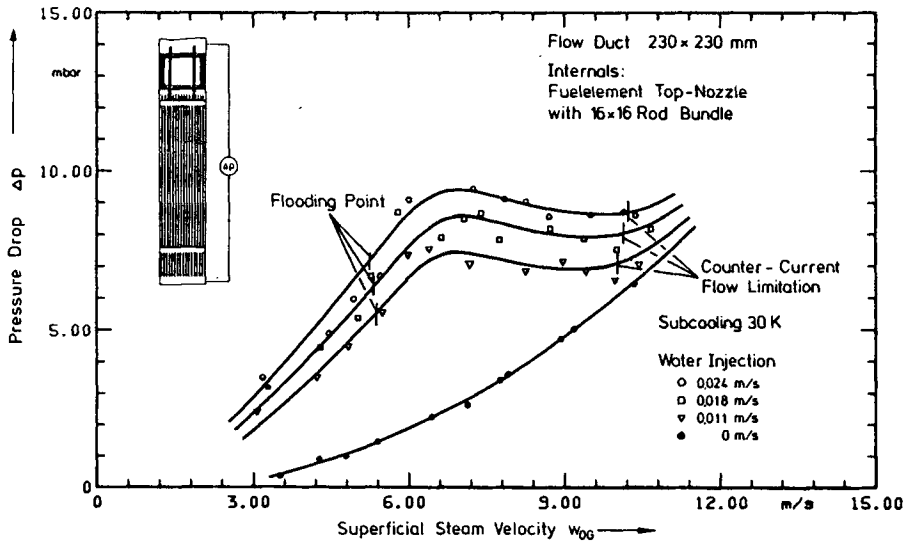

Fig. 16 Pressure drop across the rod bundle at different water injection rates